



Changes in precipitation extremes projected by a 20-km mesh global atmospheric model



Akio Kitoh ^{a,*}, Hirokazu Endo ^b

^a University of Tsukuba, Tsukuba, Ibaraki 305-8572, Japan

^b Meteorological Research Institute, Tsukuba, Ibaraki 305-0052, Japan

ARTICLE INFO

Article history:

Received 25 June 2015

Received in revised form

25 August 2015

Accepted 5 September 2015

Available online 14 September 2015

Keywords:

Heavy precipitation

Climate change

High-resolution

GCM

ABSTRACT

High-resolution modeling is necessary to project weather and climate extremes and their future changes under global warming. A global high-resolution atmospheric general circulation model with grid size about 20 km is able to reproduce climate fields as well as regional-scale phenomena such as monsoonal rainfall, tropical and extratropical cyclones, and heavy precipitation. This 20-km mesh model is applied to project future changes in weather and climate extremes at the end of the 21st century with four different spatial patterns in sea surface temperature (SST) changes: one with the mean SST changes by the 28 models of the Coupled Model Intercomparison Project Phase 5 (CMIP5) under the Representative Concentration Pathways (RCP)-8.5 scenario, and the other three obtained from a cluster analysis, in which tropical SST anomalies derived from the 28 CMIP5 models were grouped. Here we focus on future changes in regional precipitation and its extremes. Various precipitation indices averaged over the Twenty-two regional land domains are calculated. Heavy precipitation indices (maximum 5-day precipitation total and maximum 1-day precipitation total) increase in all regional domains, even where mean precipitation decrease (Southern Africa, South Europe/Mediterranean, Central America). South Asia is the domain of the largest extreme precipitation increase. In some domains, different SST patterns result in large precipitation changes, possibly related to changes in large-scale circulations in the tropical Pacific.

© 2015 The Authors. Published by Elsevier B.V. This is an open access article under the CC BY license (<http://creativecommons.org/licenses/by/4.0/>).

1. Introduction

Both too much water and too little water are of great concern for human life because the contrasts in precipitation between wet and dry regions and between wet and dry seasons are projected to increase in a coming future world (Intergovernmental Panel on Climate Change (IPCC), 2013). Warmer climate should theoretically lead to more precipitation extremes due to increasing atmospheric water vapor content (Allen and Ingram, 2002; Allan and Soden, 2008). The intensity of precipitation extremes, however, depends on not only water vapor content but also on atmospheric environmental changes (O’Gorman and Schneider, 2009). Based on global climate model (GCM) simulations of the Coupled Model Intercomparison Project Phase 3 (CMIP3, Meehl et al., 2007), it is assessed that the frequency of heavy precipitation or the proportion of total rainfall from heavy rainfalls will likely increase in the 21st century over many areas of the globe (IPCC, 2012). The same

assessment was made with the CMIP5 (Taylor et al., 2012) models under Representative Concentration Pathways (RCPs) such that extreme precipitation events over most of the mid-latitude land masses and over wet tropical regions will very likely become more intense and more frequent by the end of this century, as global mean surface temperature increases (IPCC, 2013).

The CMIP5 models have better performance than the previous CMIP3 models in simulating precipitation extremes in the present climate (Sillmann et al., 2013a). A part of this improvement may come from increasing horizontal resolution, about 280 km in CMIP3 versus about 200 km in CMIP5. Spatial distribution of precipitation indices is reasonably reproduced but differences are still found in precipitation intensity where the magnitude of precipitation extremes is underestimated by climate models (Sillmann et al., 2013a; Mehran et al., 2014).

In a future warming world, change rate of heavy precipitation amounts will generally increase more than that of annual mean precipitation (Tebaldi et al., 2006; Sun et al., 2007; Sillmann et al., 2013b). The increasing rate of annual mean precipitation at the end of the 21st century projected by CMIP5 models in RCP8.5 scenario is 9% (median value), while that in simple daily intensity

* Correspondence to: Faculty of Life and Environmental Sciences, University of Tsukuba, 1-1-1 Tennodai, Tsukuba, Ibaraki 305-8572, Japan.

E-mail address: kito.akio.ff@u.tsukuba.ac.jp (A. Kitoh).

index (SDII) defined as annual total precipitation divided by the number of wet days is 12% and that in annual maximum 5-day precipitation total (R5d) is 20% (Sillmann et al., 2013b). This increasing rate depends on the scenario, where the change ratio of R5d is 6% in RCP2.6 and 10% in RCP4.5, respectively. Similarly, 20-year or 50-year return values of daily precipitation are projected to increase and 20-year or 50-year return periods for the present precipitation events will reduce in the future almost everywhere except for subtropical dry regions (Kharin et al., 2013; Toreti et al., 2013). The 20-year return values increase about 6% per a degree change in annual mean surface temperature, but with considerable inter-model variability (Kharin et al., 2013). Large variability is also known among models in simulated increase of precipitation extremes, particularly in summer when organized convection matters (Toreti et al., 2013).

Both thermodynamical and dynamical factors are responsible for regional precipitation changes, with the former dominating the latter for extreme precipitation changes (Emori and Brown, 2005). Increase in maximum atmospheric water vapor due to temperature rise is a principal factor for increasing the intensity of individual precipitation events (Kunkel et al., 2013). There are additional factors such as changes in updrafts, which controls changes in moisture flux convergence, and soil moisture over land. Representation of precipitation, particularly its intensity, depends on the horizontal resolution of models. Coarse horizontal resolution of GCMs tends to prevent simulating realistic extreme events (Sun et al., 2006; Min et al., 2011). High-resolution modeling or statistical downscaling is then necessary to project weather and climate extremes and their future changes under global warming.

Dynamical downscaling is able to simulate more realistic, though not perfect, extreme events. Regional climate models (RCMs) would add values on more realistic topography and lower boundary conditions and better representation of dynamical processes (e.g., Takayabu et al., 2015). Therefore RCMs are widely used to project future changes in extremes. For example, Fowler et al. (2007) used six RCMs integrations under the SRES A2 scenario to downscale extreme precipitation changes over Europe at the end of the 21st century. Horizontal resolution of these RCMs is about 50 km. They found that all RCMs project increases in magnitude of extreme precipitation from 1-day to 10-day duration for most of Europe. It is also found that the magnitude of change is influenced by the driving GCMs but projected scatter is moderated by the RCM probably due to better representation of extreme events in RCM. RCMs also give different spatial pattern of precipitation extremes than that obtained by parent GCMs.

Another way for downscaling is to use an atmospheric general circulation model (AGCM) with horizontally high-resolution (Kitoh et al., 2009, 2015). Higher resolution model is needed to better reproduce precipitation climatology such as the East Asia summer rain band (Kitoh and Kusunoki, 2008), over India (Rajendran et al., 2013), South America (Kitoh et al., 2011), Central America and the Caribbean (Nakaegawa et al., 2014). Kamiguchi et al. (2006) analyzed future changes of precipitation indices between the present climate and the future climate at the end of the 21st century under the IPCC Special Report on Emission Scenario (SRES) A1B scenario by two 10-year simulations with the global 20-km mesh AGCM developed at the Meteorological Research Institute (MRI) version 3.1 (MRI-AGCM3.1, Mizuta et al., 2006). They found significantly increased heavy precipitation in South Asia, the Amazon and West Africa. Over the Amazon, an increase in dry spell is found during the dry season in the future, which is related to the Walker circulation changes associated with the El Niño-like SST changes in the future.

The MRI-AGCM has been updated recently (MRI-AGCM3.2, Mizuta et al., 2012), which improved heavy precipitation climatology around the tropical western Pacific and the global

distribution of tropical cyclones (Murakami et al., 2012). In this paper, after evaluating the present-day precipitation extremes of 20-km mesh MRI-AGCM3.2, we analyze projected future changes in precipitation extremes at the end of the 21st century. The scenario is based on RCP8.5, and four different spatial patterns in sea surface temperature (SST) changes are used as boundary conditions. This type of simulations, which uses the observed present-day interannually varying SST plus ensemble mean future SST changes obtained by CMIP-class models, can minimize the effects of climate model bias (Kitoh et al., 2015). In particular, the 20-km mesh MRI-AGCM has superiority in reproducing precipitation extremes in its present-day experiments; the results obtained in the future climate projections can be used widely for impact studies from future changes of extremes.

2. Model and experiment

2.1. MRI AGCM

We used the MRI-AGCM3.2 (Mizuta et al., 2012), which is the updated version from the MRI-AGCM3.1 (Mizuta et al., 2006). The model is based on a hydrostatic primitive equation system using a spectral transform method of spherical harmonics. The 20-km mesh version uses a triangular truncation at wave number 959 (TL959) in the horizontal, which has 1920 × 960 grid points. There are 64 layers in the vertical with a top at 0.01 hPa. A two-time-level semi-implicit semi-Lagrangian scheme is employed for time integration. For cumulus parameterization scheme, a new mass-flux type scheme (Yoshimura et al., 2015) is used. This Yoshimura scheme is based on Tiedtke (1989) scheme with a detailed entraining and detraining plume within a single grid cell, but also allows multiple convective updrafts with different heights to exist as with the Arakawa-Schubert (1974) type scheme. Prognostic variables include cloud water and cloud amount. The radiation code considers absorptions by greenhouse gases in the long wave scheme. The direct effect of aerosol (sulfate, black carbon, organic carbon, mineral dust, and sea salt) is included, but indirect effects are not considered in this experiment.

2.2. Experiment method

We have conducted the Atmospheric Model Intercomparison Project (AMIP)-type simulations for the present climate (1979–2003) and the future climate at the end of the 21st century (2075–2099). The present climate simulation used the observed interannually varying monthly mean SST and sea-ice concentration during 1979–2003 based on the HadISST1.1 data (Rayner et al., 2003). For the future climate, the boundary SST data were prepared by superposing the future change in the multi-model ensemble of SST projected by CMIP5 multi-model dataset to the present-day observed SST. In short, the future SST is the sum of (i) the trend in the multi-model ensemble (MME) of SST projected by CMIP5 multi-model dataset, (ii) future change in MME of SST for 2075–2099 and (iii) de-trended observed SST for the period 1979–2003. See Mizuta et al. (2008, 2014) for the details. Fig. 1a shows the annual mean SST changes of the 28 CMIP5 models. It is noted that there is a large contrast in SST warming between the Northern Hemisphere and the Southern Hemisphere, with the former warming more than the latter. In the tropics, relatively larger warming is noted in the central and eastern equatorial Pacific. Over the Indian Ocean, a warming in the western Indian Ocean is larger than that in the eastern Indian Ocean.

In order to assess the uncertainty in projections, we made three other simulations with different SST spatial patterns in the future. Three SST patterns are obtained by a cluster analysis of 28 CMIP5

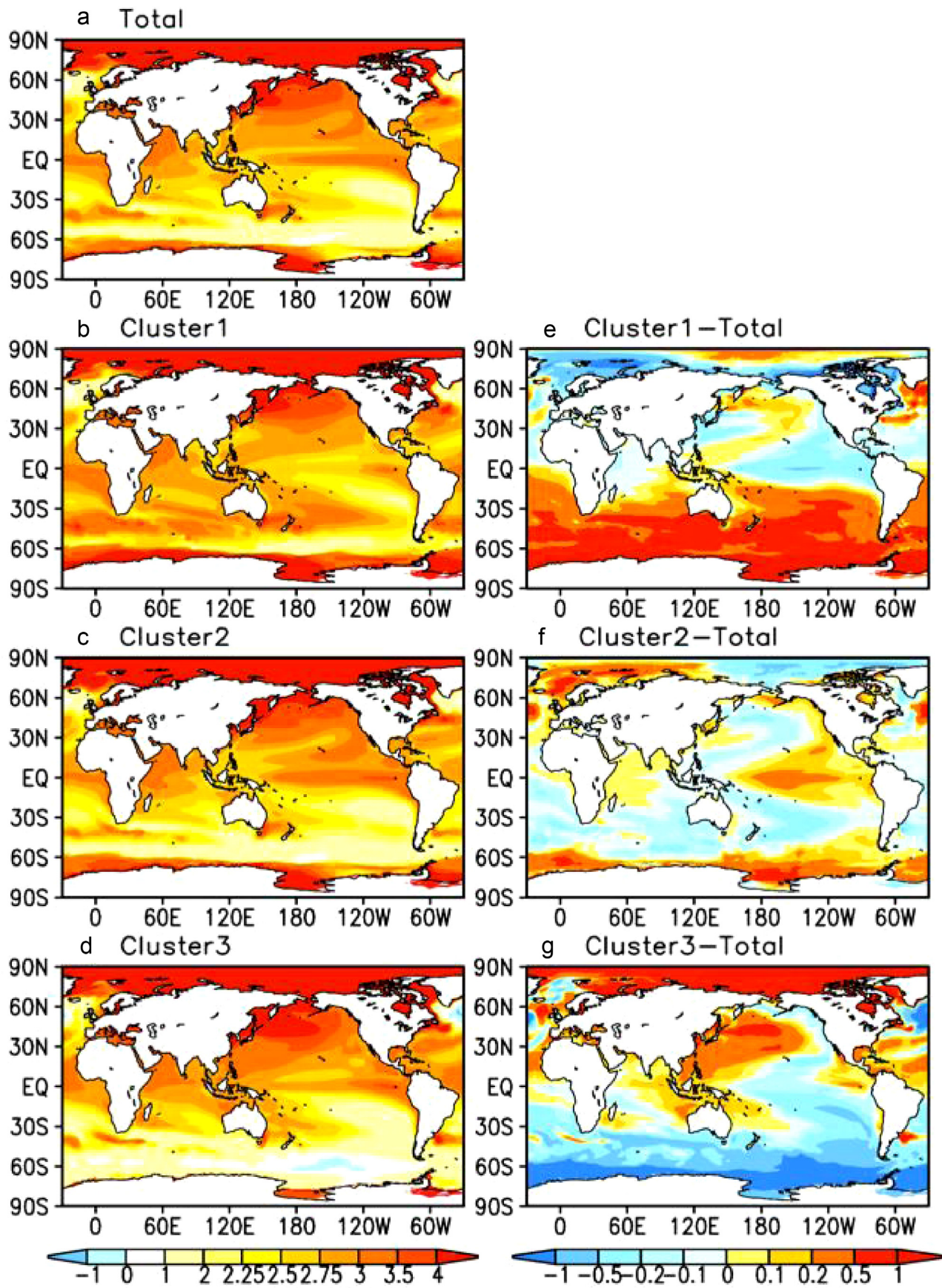


Fig. 1. Annual-mean sea surface temperature changes (K) between the present (1979–2003 average, historical experiment) and the end of the 21st century (2075–2009 average, RCP 8.5 experiment), for (a) the composite of total 28 models, and (b, c, d) the composites of the three clusters of the models. (e, f, g) Differences for each cluster from the total mean.

RCP8.5 experiments (Mizuta et al., 2014), and are shown in Fig. 1. In a clustering procedure, an equal weight is given in all 28 models. Values are normalized so that the tropical (30°S to 30°N) mean SST changes from the present (1979–2003 of historical experiment) to the end of the 21st century (2075–2099 of RCP8.5 experiment) become the same as that in the total 28 models mean. Then clustering is performed using normalized tropical SST changes because the effect of tropical SST should be larger than that of the mid- to high-latitude oceans. The clustering is finished when the final three clusters are obtained. Finally, 8, 14, and 6 models are classified as Cluster 1, Cluster 2, and Cluster 3, respectively. Cluster 1 is characterized by a nearly uniform warming in the both hemispheres, while cluster 3 is dominated by a larger warming in the Northern Hemisphere than in the Southern Hemisphere. Cluster 2 shows a larger warming over the central equatorial Pacific (so-called El Niño-like pattern). The CMIP5 models tend to show greater precipitation increases over larger SST warming (“warmer-get-wetter” pattern). These characteristics of the three clusters are discussed in Mizuta et al. (2014).

For the present climate experiment, we have performed two simulations with different initial conditions. For the future, four member simulations with different SST patterns were performed. Initial conditions are arbitrarily chosen from a previous long-term climate simulation because memory of atmospheric initial conditions is lost within a month or so. A few months spin-up simulation is performed before starting the main integration period. In this study, we use the averages of two members for the present (50 years total), and the averages of four members for the future (100 years total). Sensitivity to different SST forcing on regional precipitation changes is also discussed. The annual mean SST changes between the present (1979–2003 mean) and the future (2075–2099 mean) averaged in the tropics (30°S to 30°N) is set to 2.74 °C, which is the average of 28 CMIP5 models of the RCP8.5 experiments (Mizuta et al., 2014). Simulated global annual mean surface air temperature changes by the MRI-AGCM3.2 between the present and the future is 3.49 °C.

2.3. Observed data

For verification of the simulated precipitation, we used two observed dataset. One is the 0.25-degree resolution TRMM-3B42V7 (Huffman et al., 2007) for the period 1998–2013. The other is the GPCP-1DD v.1.2 of the Global Precipitation Climatology Project (GPCP) with a 1-degree by 1-degree grid (Huffman and Bolvin, 2009). This data set also covers 1998–2013. The data period is different between the observed data and the model simulation, but does not affect our study as we investigate climatological statistics.

2.4. Data processing

We used five precipitation indices, out of which four extreme precipitation indices are the ones suggested by the Expert Team on Climate Change Detection and Indices (ETCCDI; Klein Tank et al., 2009), as shown in Table 1: average precipitation (Pav), simple precipitation daily intensity index (SDII), annual maximum 5-day precipitation total (R5d), annual maximum 1-day precipitation total (R1d), and annual maximum consecutive dry days (CDD).

All the precipitation indices for the observations and models are calculated on their original grid. In addition, precipitation indices calculated from model data spatially averaged into 1-degree by 1-degree boxes are also calculated to check their resolution dependency.

Regional analysis is performed over the twenty-two land sub-regions used in the IPCC Fourth Assessment Report (Christensen et al., 2007), as shown in Fig. 2. For calculation of the regional

Table 1
Definition of the precipitation extreme indices.

Index	Unit	Definition
Pav	mm/day	Annual mean precipitation
SDII	mm/day	Simple daily intensity index: Annual total precipitation divided by the number of wet days (daily precipitation ≥ 1 mm)
R5d	mm	Annual maximum 5-day precipitation total
R1d	mm	Annual maximum 1-day precipitation total
CDD	day	Annual maximum number of consecutive dry days (daily precipitation < 1 mm)

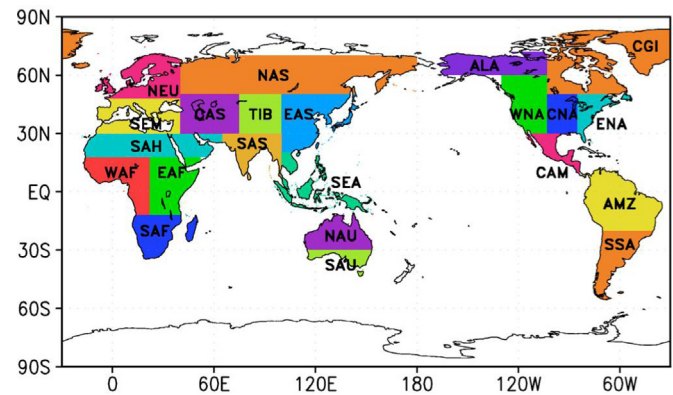


Fig. 2. Regional domain used in this study.

change ratio for the indices, the indices on their original grid are averaged for different regions for the present (1979–2003) and the future (2075–2099), and then the changes in the regionally averaged indices are divided by the corresponding regionally averaged indices in the present.

3. Evaluation of present-day climate

MRI-AGCM3.2 shows a good skill in simulating dynamical and hydro-meteorological fields such as monsoon precipitation. The model also reproduces various characteristics of tropical cyclones such as their intensity and global distribution (Mizuta et al. 2012).

Here we evaluate five extreme precipitation indices, Pav, SDII, R5d, R1d and CDD, whose definition is shown in Table 1. Fig. 3 shows global distributions of these five indices based on daily precipitation data both for observations and the 20-km mesh MRI-AGCM3.2. Here extreme precipitation indices based on TRMM-3B42 are shown as 16-year averages for the period 1998–2013. We note that quantitatively there is large discrepancy in values between the two observed dataset, namely TRMM-3B42 and GPCP-1DD, where GPCP-1DD shows considerably smaller amount in precipitation extremes, as will be shown later.

The model has reproduced the annual mean precipitation (Pav) very well in its geographical pattern (Fig. 3a and f). Simulated Pav averaged for 50°S to 50°N overestimated the TRMM observations by 10%. The MRI-AGCM3.2 shows maxima in annual precipitation over the oceans, such as the western tropical Pacific, Intertropical Convergence Zone (ITCZ), South Pacific Convergence Zone (SPCZ), the Indian Ocean, and mid-latitudes to the south of Japan and to the southeast of North America. Over land the model reproduces heavy rainfall area over Amazon. The 20-km mesh high-resolution enables a narrow precipitation area along the southern periphery of Himalaya. As discussed in Mizuta et al. (2012), monsoonal seasonal migration of precipitation zones between winter and summer is also well captured.

There is quantitatively large discrepancy in simple daily

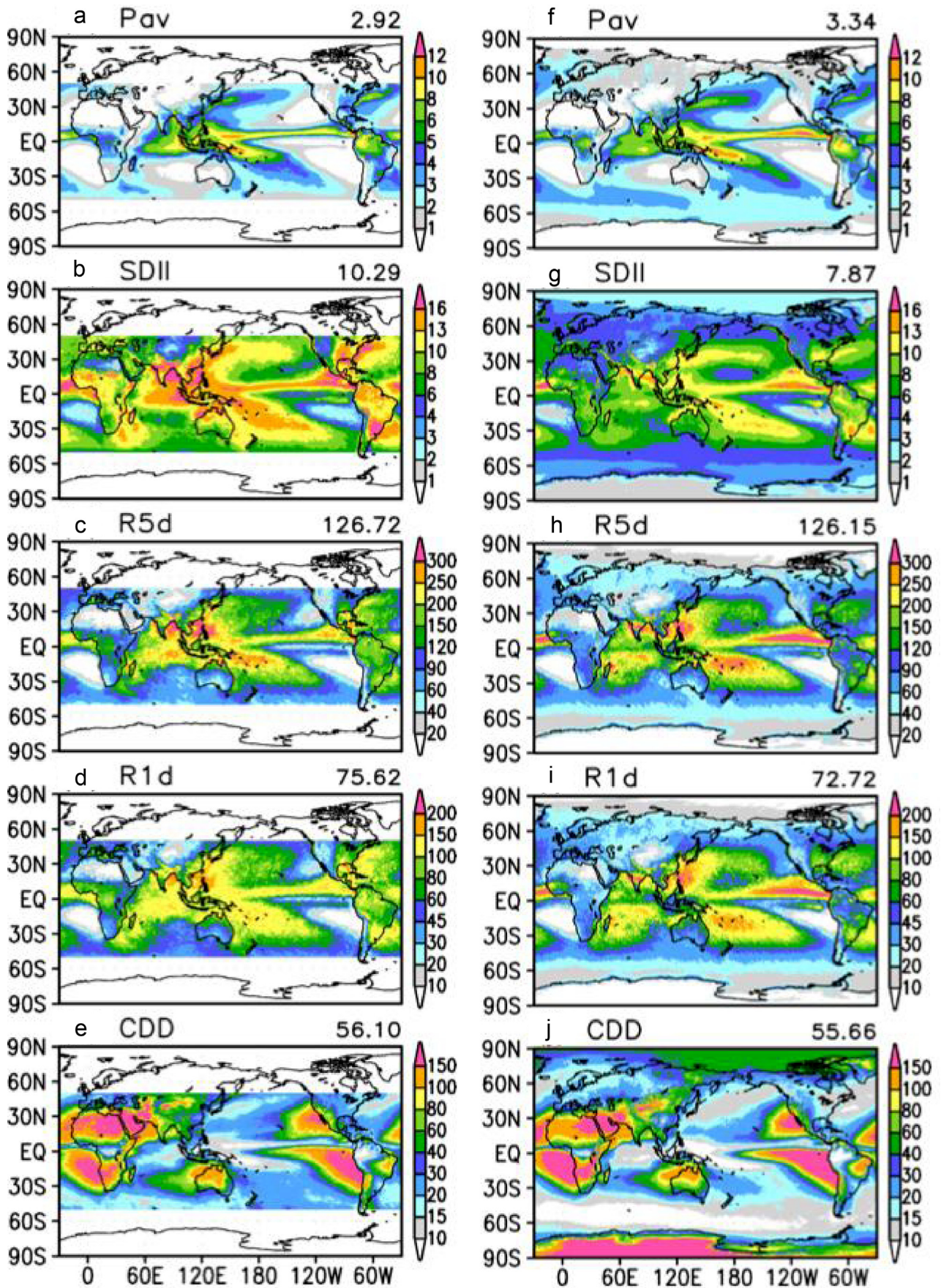


Fig. 3. (left) Observed and (right) simulated annual precipitation indices. (a, f) Pav, (b, g) SDII, (c, h) R5d, (d, i) R1d, (e, j) CDD. Observations are based on TRMM-3B42 for the period 1998–2013. See Table 1 for units. Area averages for 50°S to 50°N are shown in upper right corner of each figure.

precipitation intensity (SDII) between the model and simulations (Fig. 3b and g). The MRI-AGCM3.2 significantly (more than 20% in the 50 °S to 50 °N mean) underestimated the TRMM observations. As the annual precipitation is about 10% larger in the model, this means the number of wet days (daily precipitation ≥ 1 mm) being overestimated in the model, i.e., too many wet days with moderate-to-light precipitation (Mizuta et al. 2012). This too many drizzle-day syndrome (models produce precipitation too frequently and too lightly) is found in many GCMs (Dai, 2006; Stephens et al., 2010). This may be related to models' horizontal resolution, because precipitation is calculated for a considerably larger domain than actual precipitating clouds.

Simulated annual maximum 5-day precipitation total (R5d) and annual maximum 1-day precipitation total (R1d), on the other hand, matches well the observations (Fig. 3 c vs. h and Fig. 3d vs. 3i). However, the model overestimated both R5d and R1d over the eastern tropical Pacific. TRMM observations show the maxima over the Philippines Sea, the South China Sea, and the Bay of Bengal. The model tends to underestimate R5d and R1d over the maritime continent and at the equator.

The current model (MRI-AGCM3.2) is much better than the previous version of the model (MRI-AGCM3.1). For example, the R5d value in SAS was 104.3 mm in MRI-AGCM3.1 (Kamiguchi et al., 2006) while it is 173.6 mm in our results. As TRMM and GPCP show 184.3 mm and 157.8 mm, respectively, our model gives much closer agreement with the observations.

Fig. 3e and j shows the CDD, maximum number of consecutive dry days (daily precipitation < 1 mm). The model generally reproduces CDD well.

Fig. 4 shows the regional averages of observed and simulated annual precipitation indices. Twenty-two regional domains used in this study are shown in Fig. 2. Here we show two observations based on TRMM-3B42 and GPCP-1DD. Note that TRMM data does not cover high-latitudes. In order to check the resolution difference between the two observed datasets, simulated data re-gridded into 1-degree by 1-degree (red crosses) are also plotted together with original 20-km mesh data (black crosses). Spatial averaging into 1-degree by 1-degree causes the reduction in SDII and R1d. However, it does not affect much R5d, and very little in Pav. Differences between TRMM-3B42 and GPCP-1DD are particularly large in R1d, and larger than the differences between the original and re-gridded simulated values. This implies that the differences between TRMM-3B42 and GPCP-1DD are not solely responsible for their resolution.

Comparison of regionally averaged Pav reveals that the MRI-AGCM3.2 reproduces regional annual mean precipitation amount very well (Fig. 4a). The model tends to overestimate Pav over dry regions (SAH, CAS, ALA, CGI, WNA). In other tropical and mid-latitude wet regions, the model reproduces the observed values within 20%.

Maxima in simulated Pav are found in SEA and AMZ, followed by SAS, as in the observations. Sillmann et al. (2013a) noted that CMIP5 models underestimated the total annual precipitation in SEA and overestimated in AMZ compared with HadEX2 dataset (Donat et al., 2013). Although we are using different observations, these biases are not seen in MRI-AGCM3.2 simulations.

Fig. 4b shows the regional means of SDII. The SDII estimated by GPCP-1DD are smaller than that calculated by TRMM-3B42 in all regions where data is available. Even with this large uncertainty in the observations, simulated SDII is underestimated in almost all regions. Exceptions are found in cold regions such as ALA, CGI and WNA. Largest SDII is observed in SAS, followed by SEA, while total precipitation (Pav) is largest in SEA, not in SAS. The MRI-AGCM3.2 simulated these characteristics.

Fig. 4c and d shows the regional means of R5d and R1d. The model reproduces regional differences in these two extreme

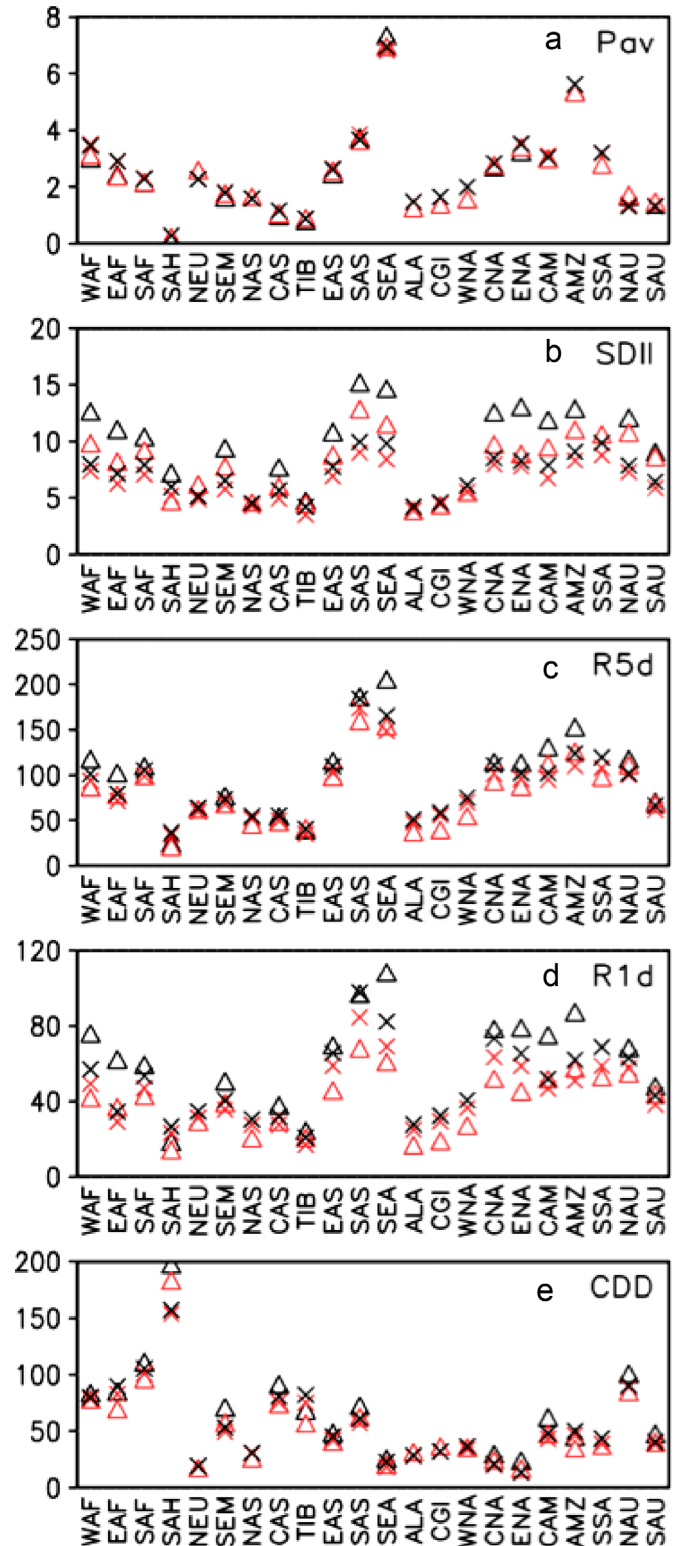


Fig. 4. Regional averages of observed and simulated annual precipitation indices in (a) Pav, (b) SDII, (c) R5d, (d) R1d, (e) CDD. Observations are based on TRMM-3B42 (black triangles) and GPCP-1DD (red triangles) for the period 1998–2013. Simulated data re-gridded into 1-degree by 1-degree (red crosses) are also plotted together with original 20-km mesh data (black crosses). (For interpretation of the references to color in this figure legend, the reader is referred to the web version of this article.)

precipitation indices, and simulated values are found in between the two observations in most areas. Maxima in R5d and R1d are located in SEA and SAS both in the observations and the model.

There are ambiguities between TRMM and GPCP, namely, the R1d maximum is in SEA followed by SAS in TRMM but in opposite order in GPCP. The MRI-AGCM3.2 simulates the R1d maximum in SAS followed by SEA.

Regional distribution of CDD is also well simulated by the MRI-AGCM3.2 (Fig. 4e). Small CDD values in SEA are noted both in the observations and model simulation. A relatively long CDD appears in SAS, where mean value as well as excessive precipitation is large.

Overall five precipitation extremes indices simulated in MRI-AGCM3.2 in its present-day climate experiment are in good agreement with those observed. In the next section, we investigate future changes in these indices at the end of the 21st century in RCP8.5 scenario.

4. Future changes in precipitation extremes

Fig. 5 shows the projected future changes in five precipitation indices at the end of the 21st century, as indicated by percent changes from the present values. The present corresponds to the average of two members for 1979–2003. The future is the average of four members for 2075–2099. Shadings denote where all four future members have the same sign of change compared to the averages of present-day simulations.

Global-scale spatial pattern of annual mean precipitation changes (Fig. 5a) is very similar to that of the CMIP5 multi-model mean assessed in IPCC (2013) and other references. Annual mean precipitation is projected to increase in the high latitudes, the equatorial Pacific Ocean and many of mid-latitude wet regions, while decrease in many mid-latitude and subtropical dry regions. This similarity, at least in its large-scale features, can be understood by the fact that our experiment strategy uses the CMIP5 multi-model mean SST changes and precipitation changes are strongly affected by SST anomalies (a warmer-get-wetter pattern; Xie et al., 2010; Chadwick et al., 2013).

Projected future changes in SDII (Fig. 5b) generally show a similar geographical pattern to that in Pav, but with smaller area in negative changes. The Mediterranean and the region to the southwest of Australia are among such areas. Area with negative future changes becomes much smaller in more extreme precipitation indices of R5d and R1d (Fig. 5c and d). Globally averaged change ratio become larger in R5d (18.72%) and more in R1d (25.70%) than that in SDII (10.42%) and Pav (7.75%). Normalized by the global annual mean surface air temperature change, they correspond to 2.22%/°C (Pav), 2.99%/°C (SDII), 5.36%/°C (R5d) and 7.36%/°C (R1d), respectively. The projected 18.72% increase in R5d for the period 2075–2099 in RCP8.5 scenario is within CMIP5 models range (Sillmann et al., 2013b). Almost all land grid points show positive changes in R5d and R1d with some exceptions near some coastal areas.

Fig. 5e shows the future changes in CDD. Annual CDD is projected to decrease in the high latitudes, eastern part of the Eurasian continent, and some oceanic areas such as the eastern equatorial Pacific. Areas with increasing CDD are much broader than where Pav decreases. This means that there are regions where annual mean precipitation is projected to increase, and at the same time the number of consecutive dry days becomes longer as already noted (IPCC, 2013).

Among the four SST clusters experiments, there are some differences in the magnitude of changes in extreme precipitation indices, although spatial patterns of precipitation changes are similar each other. It is found that the cluster 3 experiment gives the largest R1d, R5d and SDII, while the cluster 1 experiment gives the least. For example, the global mean R1d ranges from 23.95% (cluster 1) to 26.86% (cluster 3). The cluster 3 SST experiment

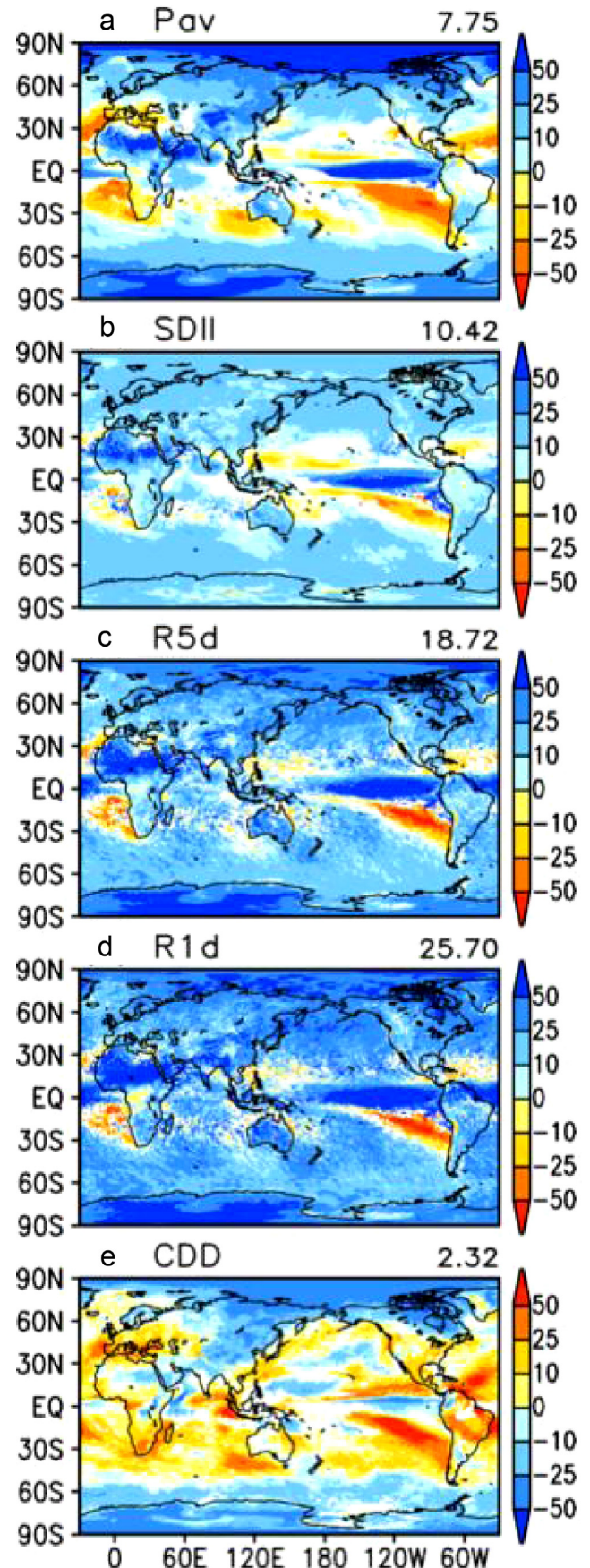


Fig. 5. Future change ratio (%) in (a) Pav, (b) SDII, (c) R5d, (d) R1d, (e) CDD. Global averages are shown in upper right corner of each figure. Shadings denote where all four future members have the same sign of the change. A spatial nine-point smooth filter is applied to reduce small-scale noise. Global average values are shown in upper right corner of each figure.

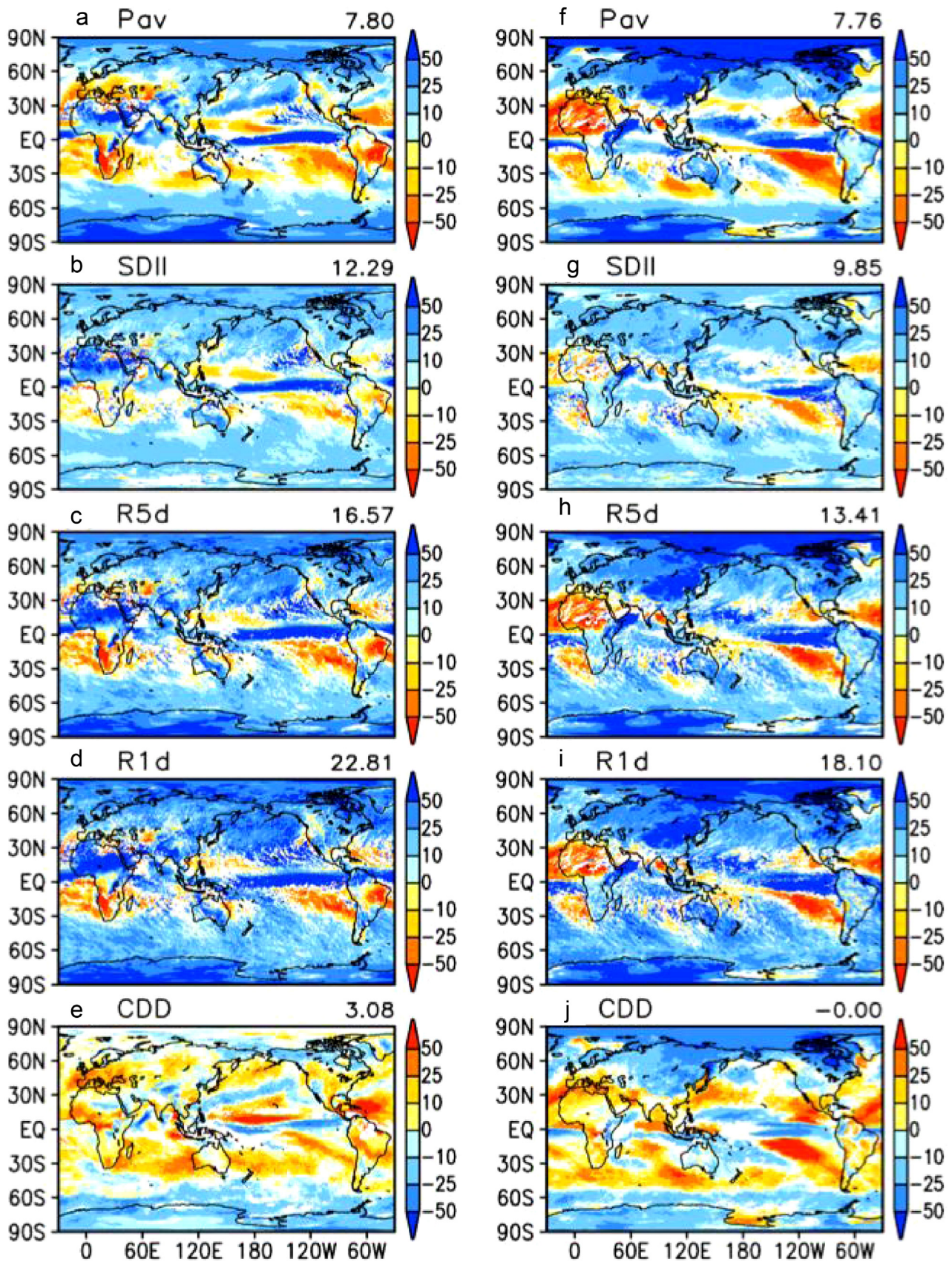


Fig. 6. As in Fig. 5 but for (a–e) June–July–August, and (f–j) December–January–February.

resulted in heaviest precipitation in the central and eastern equatorial Pacific. It should be noted that uncertainty in future SST change pattern results in some quantitative differences.

Fig. 6 shows the percent changes in the five precipitation indices but for June–July–August (JJA) and December–January–February (DJF) seasons. Changes in Pav are again generally similar to CMIP5 results. Seasonal shift of projected changes is seen. Negative Pav anomalies cover whole Europe in JJA, while they are found in the Mediterranean region and North Africa in DJF. In South Africa,

negative precipitation changes are projected in JJA season. In wintertime northern America, negative Pav anomalies are projected in southwestern US and Mexico. Over Amazon, precipitation will increase in summer (DJF), but decrease in winter (JJA).

The above contrast between summer and winter can also be seen in SDII, R5d and R1d in the low-latitudes where extremely large precipitation is projected to increase in the summer hemisphere land regions, and decrease in the winter hemisphere. The changes with opposite sign to CMIP5 projections are seen in the

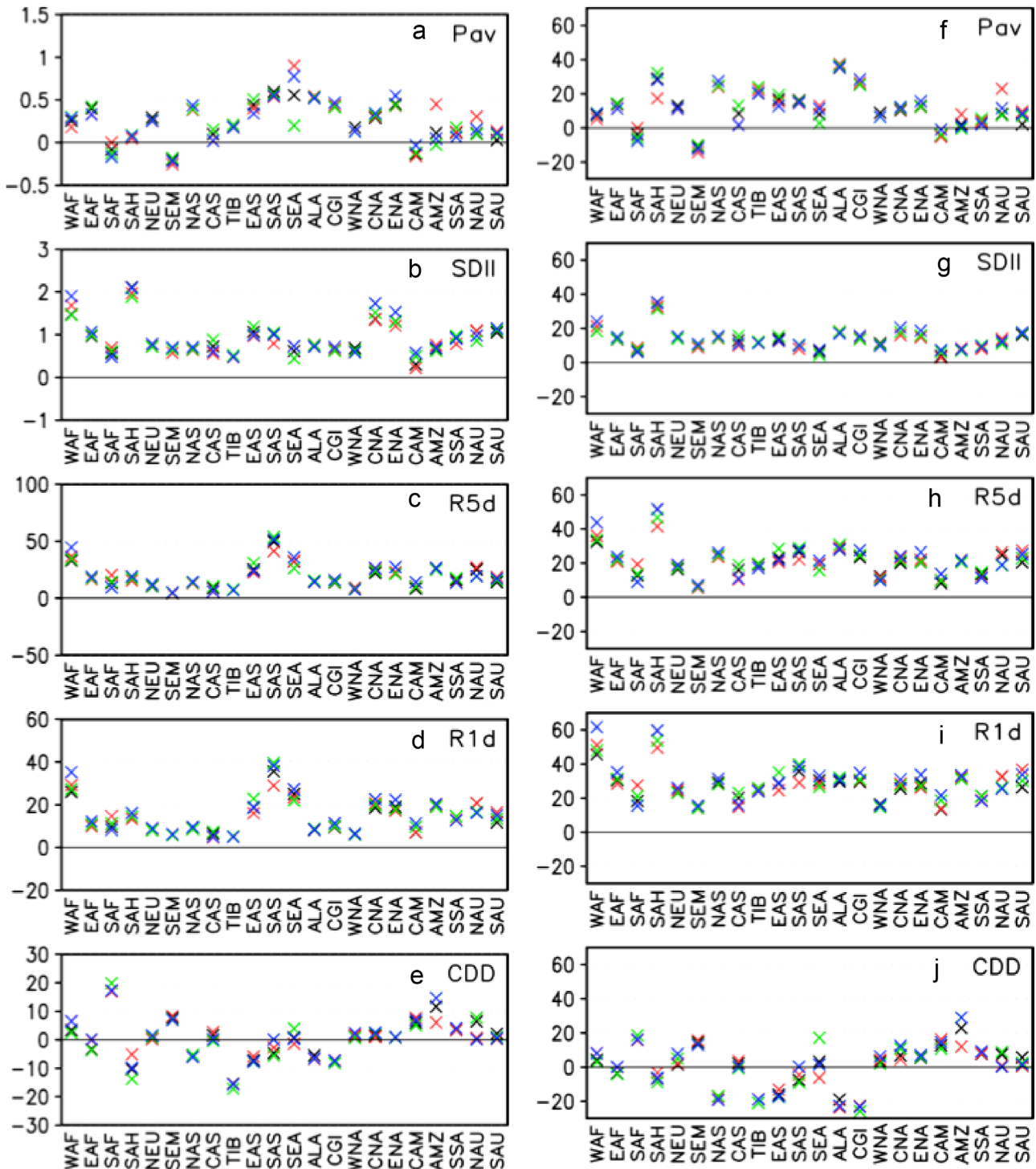


Fig. 7. Future changes of regionally averaged precipitation indices (a–e) and their change ratio (%) (f–j). Projections using the future SST pattern of the 28 CMIP5 multi-model mean, cluster 1, cluster 2, and cluster 3 are represented in black, red, green, and blue, respectively. (For interpretation of the references to color in this figure legend, the reader is referred to the web version of this article.)

western tropical Pacific where SDII, R5d and R1d are projected to decrease in summer (JJA). Importance of coupled ocean–atmosphere process in the western tropical Pacific is demonstrated for seasonal prediction because atmospheric feedback on SST is critical in this region (Wang et al., 2005). Therefore, disagreement projected precipitation changes between the CMIP5 models and our experiment can be due to our experiment setting where we used fixed SST as lower boundary conditions. Large percentage changes appear in some dry regions such as Sahara due to very little precipitation in the present climate. CDD is projected to increase in northern summer in Europe, north Asia and North America.

Next we investigate future changes in regional average annual precipitation indices (Fig. 7). As we have made four members simulations for the future climate projections with different SST patterns, all four results are shown to check uncertainty of future regional precipitation extremes projections.

Fig. 7a shows the regionally averaged annual mean precipitation changes between the end of the 21st century and present, while Fig. 7b shows the percent change ratio. Annual mean precipitation (Pav) is projected to increase in almost all land domains, but it is projected to decrease in SAF, SEM and CAM. Regions with most consistent changes in Pav are SAS, ALA and CGI where standard deviation among four realizations is less than 10% of the ensemble mean changes. Large scatter among four realizations is found in AMZ, CAS, SAF, NAU and SEA. In some of the above domains, different SST patterns used have resulted in large precipitation changes, possibly related to large-scale circulation changes in the tropical Pacific. In AMZ, even sign of Pav change is different among realizations where the experiment with the cluster 2 SST shows decreased Pav while other members show increased Pav. The cluster 2 SST has a larger SST warming in the central and eastern tropical Pacific. This strong El Niño-like SST pattern may have resulted in precipitation decrease, which is consistent with the fact that in interannual time scale Amazon tends to have less precipitation in El Niño years. The SAF is also affected much by the SST patterns used. The cluster 1 SST has a large warming around South Africa than other clusters. Experiments with other SST clusters resulted in a Pav decrease in SAF, while warmer SST in the cluster 1 SST resulted in near zero precipitation changes.

Large positive Pav changes in magnitude are projected in SEA and SAS. Scatter among four experiments is large in SEA, where the experiment with the cluster 2 SST shows least positive Pav increase. Large positive ratio changes are shown in cold regions in high latitudes (ALA, CGI, NAS) and high mountain area (TIB).

Heavy precipitation indices (SDII, R5d, R1d) increase in all regional domains, even where mean precipitation decrease (SAF, SEM, CAM). SAS is the domain of the largest extreme precipitation (R5d and R1d) increase, followed by WAF, SEA, ENA, CNA and AMZ. SEM is the domain of the least increase in R5d.

It is noted that the largest SDII increase rate in SAH is due to a large increase rate in Pav while an almost no change in the number of wet days (daily precipitation amount ≥ 1 mm), which is distinct in the summer season (not shown). WAF and SAH are the domains of largest ratio increases in R5d and R1d. Scatter among experiments in R1d and R5d is relatively small in SEA. This is in contrast to Pav, in which SEA shows large uncertainty among experiments.

Large increases in CDD are projected in SAF, AMZ, SEM and CAM. A projected increase in dry days over Amazon is consistent with Kamiguchi et al. (2006) who used the MRI-AGCM3.1 with SRES A1B multi-model mean SST anomalies. In our study, though, there are large scatter in AMZ among experiments associated with north-south contrast of future SST changes. Projected increase in CDD over Amazon is longest in cluster 3 where the Northern

Hemisphere SST warms more than the Southern Hemisphere SST. More northward shift of ITCZ over the tropical Atlantic Ocean in cluster 3 may have resulted in a longer spell of dry period in Amazon.

On the other hand, large decreases in CDD are projected in TIB, SAH, CGI, EAS, ALA and NAS. In EAS, a decrease in CDD mainly comes from wetter condition in winter (Fig. 6).

As already noted, general tendency of future precipitation extremes projected by MRI-AGCM3.2 is consistent with CMIP3 and CMIP5 multi-model ensembles. However, inter-model variability is large in some regional domains. For example, model agreement in R5d changes is less in SAH and CAM in CMIP5 model, in which more than a quarter of models projects changes in opposite signs (Sillmann et al., 2013b). Uncertainty becomes larger in CDD changes (Sillmann et al., 2013b), being consistent with our results. Our result is generally consistent with the former findings with the MRI-AGCM3.1 (Kamiguchi et al., 2006) although quantitative differences exist due to model improvement and different scenarios used.

5. Concluding remarks

In this paper, we used the four-member ensemble simulation with the global 20-km mesh AGCM at the end of the 21st century (2075–2099) under the RCP8.5 scenario. The present-day climate simulation showed good correspondence in magnitude of precipitation extremes indices such as R5d as compared with the observed estimates. A high spatial resolution of the model enabled the reproducibility of various weather systems (Oouchi et al., 2006; Murakami and Sugi, 2010), but updated physics such as cumulus parameterization improved it quantitatively (Mizuta et al., 2012; Murakami et al., 2012). Projected changes are shown in Murakami et al. (2012).

Spatial patterns of projected future changes in precipitation extremes are generally similar to that of annual mean precipitation, but area with decreasing becomes much smaller in more extreme precipitation indices of R5d and R1d. Globally averaged change ratio, normalized by the global annual mean surface air temperature change, is found to become larger in R5d (5.36%/°C) and more in R1d (7.36%/°C) than that in SDII (2.99%/°C) and Pav (2.22%/°C).

For the future projection we used four different SST change patterns derived from CMIP5 model projections (Mizuta et al., 2014). It is found that some regions are strongly affected by SST patterns. For the Pav changes, largest variability is found in Southeast Asia for its magnitude, and in Amazon for its ratio change. Amazon is the only regional domain where some member experiment yielded different signs in changes. For R5d, South Asia is the domain with largest increase in magnitude. Large scatter among experiments is found in CDD. In this paper, we did not perform detailed analysis of atmospheric circulation changes associated with different SST change patterns. This definitely should be a future work.

In this experimental setting, we only covered some uncertainty coming from future SST change patterns. The different model physics is another source for uncertainty in future climate projections. Endo et al. (2012) had performed such an attempt and showed that large uncertainty in future precipitation projections in South Asia and Southeast Asia come from differences in model physics such as cumulus convection schemes.

We have made four ensemble experiments for future projections, which is not enough to cover uncertainty range and to get probabilistic regional climate information. About dozens or 100 realizations may be needed to achieve such climate change information. The 20-km mesh GCM is too heavy to perform many

realizations. Instead we use the 60-km mesh version of the same model for ensemble experiments with many members. Although the 60-km mesh model itself has some limitation to quantitatively reproduce tropical cyclone intensity, some precipitation extremes are reasonably simulated (Endo et al., 2012). Therefore, a use of both 20-km and 60-km models would deliver meaningful information.

In our experimental setting, SST is prescribed as lower boundary conditions in the present and future simulations. The absence of air–sea interaction can cause distorted precipitation field and associated atmospheric circulations over certain regions such as the western tropical Pacific (Wang et al., 2005). This also may have resulted in too stronger tropical cyclones and associated precipitation and wind extremes. An introduction of air–sea interaction may remedy this problem and is under consideration.

Acknowledgments

This work was conducted under the Development of Basic Technology for Risk Information on Climate Change of the SOUSEI Program of the Ministry of Education, Culture, Sports, Science, and Technology of Japan.

References

- Allan, R.F., Soden, B.J., 2008. Atmospheric warming and the amplification of precipitation extremes. *Science* 321, 1481–1484.
- Allen, M.R., Ingram, W.J., 2002. Constraints on future changes in climate and the hydrologic cycle. *Nature* 419, 224–232.
- Arakawa, A., Schubert, W.H., 1974. Interaction of a cumulus cloud ensemble with the large-scale environment. Part I. *J. Atmos. Sci.* 31, 674–701.
- Chadwick, R., Boutle, I., Martin, G., 2013. Spatial patterns of precipitation change in CMIP5: why the rich don't get richer in the tropics. *J. Clim.* 26, 3803–3822.
- Christensen, J.H., Hewitson, B., Busuioc, A., Chen, A., Gao, X., Held, I., Jones, R., Kolli, R.K., Kwon, W.-T., Laprise, R., Magana Rueda, V., Mearns, L., Menendez, C.G., Raisanen, J., Rinke, A., Sarr, A., Whetton, P., 2007. Regional climate projections. In: Solomon, S., Qin, D., Manning, M., Chen, Z., Marquis, M., Averyt, K.B., Tignor, M., Miller, H.L. (Eds.), *Climate Change 2007: The Physical Science Basis. Contribution of Working Group I to the Fourth Assessment Report of the Intergovernmental Panel on Climate Change*. Cambridge University Press, Cambridge, United Kingdom, New York, NY, USA.
- Dai, A., 2006. Precipitation characteristics in eighteen coupled climate models. *J. Clim.* 19, 4605–4630.
- Donat, M.G., et al., 2013. Updated analyses of temperature and precipitation extreme indices since the beginning of the twentieth century: The HadEX2 dataset. *J. Geophys. Res. Atmos.* 118, 2098–2118. <http://dx.doi.org/10.1002/jgrd.50150>.
- Emori, S., Brown, S.J., 2005. Dynamic and thermodynamic changes in mean and extreme precipitation under changed climate. *Geophys. Res. Lett.* 32, L17706. <http://dx.doi.org/10.1029/2004GL022306>.
- Endo, H., Kitoh, A., Ose, T., Mizuta, R., Kusunoki, S., 2012. Future changes and uncertainties in Asian precipitation simulated by multi-physics and multi-sea surface temperature ensemble experiments with high-resolution Meteorological Research Institute atmospheric general circulation models (MRI-AGCMs). *J. Geophys. Res.* 117, D16118. <http://dx.doi.org/10.1029/2012JD017874>.
- Fowler, H.J., Ekstrom, M., Blenkinsop, S., Smith, A.P., 2007. Estimating change in extreme European precipitation using a multimodel ensemble. *J. Geophys. Res.* 112, D18104. <http://dx.doi.org/10.1029/2007JD008619>.
- Huffman, G.J., D.T., Bolvin, 2009. GPCP One-degree Daily Precipitation Data Set Documentation. <ftp://precip.gsfc.nasa.gov/pub/1dd-v1.1/1DD_v1.1_doc.pdf>.
- Huffman, G.J., Adler, R.F., Bolvin, D.T., Gu, G., Nelkin, E.J., Bowman, K.P., Hong, Y., Stocker, E.F., Wolff, D.B., 2007. The TRMM multi-satellite precipitation analysis: Quasi-global, multi-year, combined-sensor precipitation estimates at finer scale. *J. Hydrometeorol.* 8, 38–55.
- IPCC, 2012. Managing the risks of extreme events and disasters to advance climate change adaptation. In: Field, C.B., Barros, V., Stocker, T.F., Qin, D., Dokken, D.J., Ebi, K.L., Mastrandrea, M.D., Mach, K.J., Plattner, G.-K., Allen, S.K., Tignor, M., Midgley, P.M. (Eds.), *A Special Report of Working Group I and II of the Intergovernmental Panel on Climate Change*. Cambridge University Press, Cambridge, UK, New York, NY, USA (582 pp.).
- IPCC, 2013. Climate change 2013: the physical science basis. In: Stocker, T.F., Qin, D., Plattner, G.-K., Tignor, M., Allen, S.K., Boschung, J., Nauels, A., Xia, Y., Bex, V., Midgley, P.M. (Eds.), *Contribution of Working Group I to the Fifth Assessment Report of the Intergovernmental Panel on Climate Change*. Cambridge University Press, Cambridge, United Kingdom, New York, NY, USA (<http://dx.doi.org/10.1017/CBO9781107415324> (1535 pp.)).
- Kamiguchi, K., Kitoh, A., Uchiyama, T., Mizuta, R., Noda, A., 2006. Changes in precipitation-based extremes indices due to global warming projected by a global 20-km-mesh atmospheric model. *SOLA* 2, 64–67. <http://dx.doi.org/10.2151/sola.2006-017>.
- Kharin, V.V., Zwiers, F.W., Zhang, X., Wehner, M., 2013. Changes in temperature and precipitation extremes in the CMIP5 ensemble. *Clim. Change* 119, 345–357. <http://dx.doi.org/10.1007/s10584-013-0705-8>.
- Kitoh, A., Kusunoki, S., 2008. East Asian summer monsoon simulation by a 20-km mesh AGCM. *Clim. Dyn.* 31, 389–401. <http://dx.doi.org/10.1007/s00382-007-0285-2>.
- Kitoh, A., Ose, T., Kurihara, K., Kusunoki, S., Sugi, M., KAKUSHIN Team-3 Modeling Group, 2009. Projection of changes in future weather extremes using super-high-resolution global and regional atmospheric models in the KAKUSHIN Program: Results of preliminary experiments. *Hydrol. Res. Lett.* 3, 49–53. <http://dx.doi.org/10.3178/hr.3.49>.
- Kitoh, A., Kusunoki, S., Nakaegawa, T., 2011. Climate change projections over South America in the late 21st century with the 20 and 60 km mesh Meteorological Research Institute atmospheric general circulation model (MRI-AGCM). *J. Geophys. Res.* 116. <http://dx.doi.org/10.1029/2010JD014920>, D06105.
- Kitoh, A., Ose, T., Takayabu, I., 2015. Dynamical downscaling for climate projection with high-resolution MRI AGCM-RCM. *J. Meteorol. Soc. Jpn.* . <http://dx.doi.org/10.2151/jmsj.2015-022>
- Klein Tank, A.M.G., Zwiers F.W., Zhang X., 2009. Guidelines on Analysis of Extremes in a Changing Climate in Support of Informed Decisions for Adaptation. WCDMP-No.72, WMO-TD No.1500, (56 pp).
- Kunkel, K.E., Karl, T.R., Easterling, D.R., Redmond, K., Young, J., Yin, X., Hennon, P., 2013. Probable maximum precipitation (PMP) and climate change. *Geophys. Res. Lett.* 40, 1402–1408. <http://dx.doi.org/10.1002/grl.50334>.
- Meehl, G.A., Covey, C., Delworth, T., Latif, M., McAvaney, B., Mitchell, J.F.B., Stouffer, R.J., Taylor, K.E., 2007. The WCRP CMIP3 multi-model dataset: a new era in climate change research. *Bull. Am. Meteorol. Soc.* 88, 1383–1394.
- Mehran, A., AghaKouchak, A., Phillips, T.J., 2014. Evaluation of CMIP5 continental precipitation simulations relative to satellite-based gauge-adjusted observations. *J. Geophys. Res. Atmos.* 119, 1695–1707. <http://dx.doi.org/10.1002/2013JD021152>.
- Min, S.K., Zhang, X., Zwiers, F.W., Hegerl, G.C., 2011. Human contribution to more-intense precipitation extremes. *Nature* 470, 378–381.
- Mizuta, R., Oouchi, K., Yoshimura, H., Noda, A., Katayama, K., Yukimoto, S., Hosaka, M., Kusunoki, S., Kawai, H., Nakagawa, M., 2006. 20-km-mesh global climate simulations using JMA-GSM model – Mean climate states. *J. Meteorol. Soc. Jpn.* 84, 165–185. <http://dx.doi.org/10.2151/jmsj.84.165>.
- Mizuta, R., Adachi, Y., Yukimoto, S., Kusunoki, S., 2008. Estimation of future distribution of sea surface temperature and sea ice using CMIP3 multi-model ensemble mean. *Tech. Rep. Meteorol. Res. Inst.* 56, 28.
- Mizuta, R., Yoshimura, H., Murakami, H., Matsueda, M., Endo, H., Ose, T., Kamiguchi, K., Hosaka, M., Sugi, M., Yukimoto, S., Kusunoki, S., Kitoh, A., 2012. Climate simulations using MRI-AGCM3.2 with 20-km grid. *J. Meteorol. Soc. Jpn.* 90A, 233–258. <http://dx.doi.org/10.2151/jmsj.2012-A12>.
- Mizuta, R., Arakawa, O., Ose, T., Kusunoki, S., Endo, H., Kitoh, A., 2014. Classification of CMIP5 future climate responses by the tropical sea surface temperature changes. *SOLA* 10, 167–171. <http://dx.doi.org/10.2151/sola.2014-035>.
- Murakami, H., Sugi, M., 2010. Effect of model resolution on tropical cyclone climate projections. *SOLA* 6, 73–76. <http://dx.doi.org/10.2151/sola.2010-019>.
- Murakami, H., Wang, Y., Yoshimura, H., Mizuta, R., Sugi, M., Shindo, E., Adachi, Y., Yukimoto, S., Hosaka, M., Kusunoki, S., Ose, T., Kitoh, A., 2012. Future changes in tropical cyclone activity projected by the new high-resolution MRI-AGCM. *J. Clim.* 25, 3237–3260.
- Nakaegawa, T., Kitoh, A., Murakami, H., Kusunoki, S., 2014. Annual maximum 5-day rainfall total and maximum number of consecutive dry days over Central America and the Caribbean in the late twenty-first century projected by an atmospheric general circulation model with three different horizontal resolutions. *Theor. Appl. Climatol.* 116, 155–168. <http://dx.doi.org/10.1007/s00704-013-0934-9>.
- O’Gorman, P.A., Schneider, T., 2009. The physical basis for increases in precipitation extremes in simulations of 21st-century climate change. *Proc. Nat. Acad. Sci. USA* 106, 14773–14777.
- Oouchi, K., Yoshimura, J., Yoshimura, H., Mizuta, R., Kusunoki, S., Noda, A., 2006. Tropical cyclone climatology in a global warming climate as simulated in a 20 km-mesh global atmospheric model: frequency and wind intensity analyses. *J. Meteorol. Soc. Jpn.* 84, 259–276. <http://dx.doi.org/10.2151/JMSJ.84.259>.
- Rajendran, K., Sajani, S., Jayasankar, C.B., Kitoh, A., 2013. How dependent is climate change projection of Indian summer monsoon rainfall and extreme events on model resolution? *Curr. Sci.* 104, 1409–1418.
- Rayner, N.A., Parker, D.E., Horton, E.B., Folland, C.K., Alexander, L.V., Rowell, D.P., Kent, E.C., Kaplan, A., 2003. Global analyses of sea surface temperature, sea ice, and night marine air temperature since the late nineteenth century. *J. Geophys. Res.* 108, 4407. <http://dx.doi.org/10.1029/2002JD002670>.
- Sillmann, J., Kharin, V.V., Zhang, X., Zwiers, F.W., Bronaugh, D., 2013a. Climate extremes indices in the CMIP5 multimodel ensemble: Part 1. Model evaluation in the present climate. *J. Geophys. Res. Atmos.* 118, 1716–1733. <http://dx.doi.org/10.1002/jgrd.50203>.
- Sillmann, J., Kharin, V.V., Zwiers, F.W., Zhang, X., Bronaugh, D., 2013b. Climate extremes indices in the CMIP5 multimodel ensemble: Part 2. Future climate projections. *J. Geophys. Res. Atmos.* 118, 2473–2493. <http://dx.doi.org/10.1002/2013JD021152>.

- jgrd.50188.
- Stephens, G.L., L'Ecuyer, T., Forbes, R., Gettleman, A., Golaz, J.-C., Bodas-Salcedo, A., Suzuki, K., Gabriel, P., Haynes, J., 2010. Dreary state of precipitation in global models. *J. Geophys. Res.* 115, D24211. <http://dx.doi.org/10.1029/2010JD014532>.
- Sun, Y., Solomon, S., Dai, A., Portmann, R.W., 2006. How often does it rain? *J. Clim.* 19, 916–934.
- Sun, Y., Solomon, S., Dai, A., Portmann, R.W., 2007. How often will it rain? *J. Clim.* 20, 4801–4818.
- Takayabu, I., Kanamaru, H., Dairaku, K., Benestad, R., von Storch, H., Christensen, J. H., 2015. Reconsidering the quality and utility of downscaling. *J. Meteorol. Soc. Jpn.* (in press)
- Taylor, K.E., Stouffer, R.J., Meehl, G.A., 2012. An overview of CMIP5 and the experiment design. *Bull. Am. Meteorol. Soc.* 93, 485–498, doi:10.1175/BAMS-d-11-00094.1.
- Tebaldi, C., Hayhoe, K., Arblaster, J., Meehl, G., 2006. Going to extremes: An inter-comparison of model-simulated historical and future changes in extreme events. *Clim. Chang.* 79, 185–211. <http://dx.doi.org/10.1007/s10584-006-9051-4>.
- Tiedtke, M., 1989. A comprehensive mass flux scheme for cumulus parameterization in large-scale models. *Mon. Weather Rev.* 117, 1779–1800.
- Toreti, A., Naveau, P., Zampieri, M., Schindler, A., Scoccimarro, E., Xoplaki, E., Dijkstra, H.A., Gualdi, S., Luterbacher, J., 2013. Projections of global changes in precipitation extremes from Coupled Model Intercomparison Project Phase 5 models. *Geophys. Res. Lett.* <http://dx.doi.org/10.1002/grl.50940>
- Wang, B., Ding, Q., Fu, X., Kang, I.-S., Jin, K., Shukla, J., Doblas-Reyes, F., 2005. Fundamental challenge in simulation and prediction of summer monsoon rainfall. *Geophys. Res. Lett.* 32, L15711. <http://dx.doi.org/10.1029/2005GL022734>.
- Xie, S.-P., Deser, C., Vecchi, G.A., Ma, J., Teng, H., Wittenberg, A.T., 2010. Global warming pattern formation: sea surface temperature and rainfall. *J. Clim.* 23, 966–986.
- Yoshimura, H., Mizuta, R., Murakami, H., 2015. A spectral cumulus parameterization scheme interpolating between two convective updrafts with Semi-Lagrangian calculation of transport by compensatory subsidence. *Mon. Weather Rev.* 143, 597–621, doi:10.1175/MWR-d-14-00068.1.